THE ASTROPHYSICAL JOURNAL, 473:873–880, 1996 December 20

JET FORMATION IN INITIALLY SPHERICAL, SUPERMAGNETOSONIC MAGNETOHYDRODYNAMIC WINDS

ZHI-YUN LI[1]
Theoretical Astrophysics Center and Astronomy Department, 601 Campbell Hall, University of California, Berkeley, CA 94720; li@bkyast.berkeley.edu
Received 1995 December 11; accepted 1996 July 11

ABSTRACT

It is widely believed that outflows (or winds) from many astrophysical systems, ranging from young stellar objects to active galactic nuclei, are driven magneto-centrifugally from rapidly rotating central objects. A natural consequence of rotation and flux-freezing in such winds is that the magnetic field becomes predominantly toroidal once the flow speed exceeds the fast magnetosonic speed. We demonstrate that, because of this predominantly toroidal field, narrow jetlike density features can form spontaneously around the rotation axis of magnetohydrodynamic (MHD) winds even when their densities are initially distributed spherically. We limit our demonstration to the supermagnetosonic region where self-consistent solutions can be found by the well-known "method of characteristics." It is shown that, for nonrelativistic and modestly relativistic winds, the initially spherical isodensity contours become more and more elongated along the rotation axis, and thus more and more jetlike, on increasingly larger scales. This elongation is associated with collimation of wind streamlines by toroidal magnetic fields, although isodensity contours appear more jetlike than streamlines in general, as first noted by Shu et al. in 1995. Our concrete numerical examples support their asymptotic results that well-collimated "jets" are always surrounded by wide-angle winds and that isodensity contours could become more or less parallel to the rotation axis at large distances. We also show that formation of jetlike density features is more difficult in the supermagnetosonic region of highly relativistic MHD winds.

Subject headings: hydrodynamics — ISM: jets and outflows — MHD

1. INTRODUCTION

Straight, narrow jets are associated with many astrophysical systems, ranging from young stellar objects (e.g., Mundt 1985; Lada 1985) to active galactic nuclei (e.g., Begelman, Blandford, & Rees 1984). The spectacular, thin jets observed in the HH 30 system (Burrows et al. 1996) and Cygnus A (e.g., Carilli et al. 1996) are among the most famous examples of Galactic and extragalactic jets. One widely believed concept is that these jets are magnetohydrodynamic winds emanating from rapidly rotating central objects and collimated toward the rotation axis by the frozen-in, toroidal magnetic field (Blandford 1989; Königl & Ruden 1993). However, concrete demonstration that jets can indeed be produced in this manner is still lacking. The basic reason is the lack of general self-consistent solutions to the MHD wind equations. Although Blandford & Payne (1982) did obtain self-similar, collimated MHD wind solutions, it is not clear how the self-similarity ansatz affects the flow collimation. As a result, we still do not know whether wide-angle MHD winds emanating from a small source region can collimate themselves into narrow jets at large distances without any external support.

Based on asymptotic analyses, Heyvaerts & Norman (1989) concluded that nonrelativistic MHD winds are always well-collimated at infinity. A similar conclusion was reached by Chiueh, Li, & Begelman (1991) for relativistic ones. However, the rate for achieving this collimated state turns out to be logarithmically slow (Sakurai 1985; Begelman & Li 1994; Tomimatsu 1994; Shu et al. 1995, hereafter SNOS). The slow streamline collimation seems to undermine the concept of spontaneous jet formation in MHD winds. In fact, Eichler (1993) argued that it would be extremely difficult to collimate the majority of wind streamlines into thin jets over realistic astrophysical distance scales once the wind speed exceeds the (fast) magnetosonic speed by a moderately large factor. We demonstrate in this paper that the flow speed need not exceed the magnetosonic speed by a large factor, and that a significant fraction of the wind streamlines could become concentrated near the rotation axis over astrophysically interesting scales, and thus form a narrow "jet." The jet manifests itself most clearly in the isodensity contours, which become highly elongated along the rotation axis, as first noticed by SNOS. If emission from astrophysical outflows is biased toward high-density regions, the wind would *appear* jetlike even though a large fraction of the wind may remain non (or weakly) collimated (SNOS).

As with Heyvaerts & Norman (1989), the analysis of SNOS is limited to the asymptotic wind zone, where the MHD wind equations can be reduced to a simple enough form that, in a spherical polar coordinate system (r, θ, ϕ), a separation of variables in r and θ is possible. This enables them to tackle the problem semianalytically. In this paper, we adopt a different, but complementary approach: solving numerically for wind solutions in the super (fast) magnetosonic region. The numerical method we employ is that of Li & Shu (1996a, hereafter LS), which solves a set of simplified, steady-state MHD equations in the super (fast) magnetosonic region by the "method of characteristics," a well-known technique for studying supersonic gas dynamics (e.g., Shu 1992; Zucrow & Hoffman 1977). Motivated by the analysis of SNOS, which suggests that observable "jets" might be better traced by the isodensity contours of MHD winds (than by the streamlines), we shall follow their evolution with distance away from the source region. In particular, we want to find out whether initially *spherical* isodensity

[1] Current address: Mail code 130-33, California Institute of Technology, Pasadena, CA 91125.

contours can be distorted by the frozen-in toroidal magnetic field into jetlike shapes and, if so, how fast such a distortion (i.e., jet formation) process occurs. To this end, we organize the rest of the paper as follows: in § 2, we shall generalize LS's formulation of the supermagnetosonic MHD wind problem to include special relativistic effects. Concrete numerical examples of jet formation in both nonrelativistic and relativistic MHD winds are then given and interpreted in terms of cross-streamline force balance in § 3. A discussion of the major assumptions is also given (§ 3.4). We summarize and discuss our main results in § 4.

2. MHD WIND EQUATIONS AND THE METHOD OF CHARACTERISTICS

2.1. *Simplified Relativistic MHD Wind Equations*

Since the sound speed of the wind is usually much smaller than the Alfvén speed, we can safely neglect the thermal pressure and assume that the wind is cold. The time-independent relativistic MHD wind equations in the absence of gravity then become (e.g., Lovelace et al. 1986)

$$\nabla \cdot (\rho \boldsymbol{V}) = 0 , \tag{1}$$

$$\rho(\boldsymbol{V} \cdot \nabla)\boldsymbol{V} = \rho_e \boldsymbol{E} + \frac{1}{4\pi} (\nabla \times \boldsymbol{B}) \times \boldsymbol{B} , \tag{2}$$

$$\nabla \times \left(\frac{\boldsymbol{V} \times \boldsymbol{B}}{c\gamma} \right) = 0 , \tag{3}$$

where ρ is the proper density, $\boldsymbol{V}$ is the 4-velocity (i.e., the usual flow velocity times the Lorentz factor γ), c is the speed of light, while ρ_e, $\boldsymbol{E}$, and $\boldsymbol{B}$ are, respectively, the charge density, the electric field, and the magnetic field in the *lab* frame. The electric field and charge density are given by

$$\boldsymbol{E} = - \frac{\boldsymbol{V} \times \boldsymbol{B}}{c\gamma} , \tag{4}$$

and

$$\rho_e = \frac{\nabla \cdot \boldsymbol{E}}{4\pi} , \tag{5}$$

Since our main focus is on the collimating effect of the predominantly *toroidal* magnetic field, we shall ignore the poloidal field. It turns out that, to the same degree of approximation, the toroidal flow speed can be ignored as well (see § 3.4 below). These are reasonable approximations in the supermagnetosonic region that concerns us and, as in LS, they simplify the numerical treatment of the problem enormously.

In a cylindrical coordinate system (ϖ, ϕ, z), we can write $\boldsymbol{V} = (u\boldsymbol{e}_\varpi + v\boldsymbol{e}_z)c$ and $\boldsymbol{B} = \gamma b \boldsymbol{e}_\phi$, where b is the toroidal field strength in the *comoving frame*. Equations (1)–(3) then become

$$u\rho_\varpi + v\rho_z + \rho u_\varpi + \rho v_z + \frac{\rho u}{\varpi} = 0 , \tag{6}$$

$$\frac{b}{4\pi} (\gamma^2 - v^2) b_\varpi + \frac{b}{4\pi} (uv) b_z + \left(\rho c^2 + \frac{b^2}{4\pi} \right) u u_\varpi + \left(\rho c^2 + \frac{b^2}{4\pi} \right) v u_z + \frac{b^2}{4\pi\varpi} (\gamma^2 - v^2) = 0 , \tag{7}$$

$$\frac{b}{4\pi} (uv) b_\varpi + \frac{b}{4\pi} (\gamma^2 - u^2) b_z + \left(\rho c^2 + \frac{b^2}{4\pi} \right) u v_\varpi + \left(\rho c^2 + \frac{b^2}{4\pi} \right) v v_z + \frac{b^2}{4\pi\varpi} (uv) = 0 , \tag{8}$$

$$u b_\varpi + v b_z + b u_\varpi + b v_z = 0 , \tag{9}$$

which are the relativistic generalizations of equations (1)–(4) of LS in the cold wind limit. The subscripts in these equations denote partial derivatives.

2.2. *Characteristic Equations*

We shall follow LS in adopting the nomenclature of Shu (1992). As in the nonrelativistic case of LS, there are three different trajectory characteristics. One of them is the streamline, whose slope is given by

$$\frac{dz}{d\varpi} = \frac{v}{u} . \tag{10}$$

The other two are the Mach lines with the following slopes

$$\frac{dz}{d\varpi} = \lambda_\pm = \tan (\vartheta \pm \alpha) , \tag{11}$$

where ϑ is the angle between the instantaneous direction of the streamline and the ϖ axis and α is the Mach angle defined from $\sin \alpha = 1/M$. The (magnetic) Mach number M is the ratio of the dimensionless total flow 4-speed $V = (u^2 + v^2)^{1/2}$ and the dimensionless fast magnetosonic speed $v_f = [b^2/(4\pi\rho c^2)]^{1/2}$. Note that it is the *proper*, rather than the *lab*, toroidal field that appears in the expression for v_f. We shall refer to v_f simply as the magnetosonic speed since the slow magnetosonic speed is zero in a cold wind. It is straightforward to show from equations (6)–(9) that the solution characteristics are

$$d\left(\frac{b}{\rho\varpi} \right) = 0 , \tag{12}$$

$$d\left[\gamma \left(1 + \frac{b^2}{4\pi\rho c^2} \right) \right] = 0 , \tag{13}$$

along each streamline, and

$$\frac{\sqrt{M^2 - 1}}{M^2 [1 + b^2/(4\pi\rho c^2)]} \frac{d(b\varpi)}{b\varpi} \pm d\vartheta \mp \cos^2 \vartheta (\lambda_\pm - \tan \vartheta) \frac{d\varpi}{\varpi} = 0 , \tag{14}$$

along the Mach lines.

3. JET FORMATION IN SUPER-MAGNETOSONIC MHD WINDS

3.1. *Initial and Boundary Conditions*

Before applying the method of characteristics to construct supermagnetosonic wind solutions, we need to specify their starting and boundary conditions. For the purpose of demonstrating jet formation, we shall choose the simplest possible initial flow conditions on a sphere of given radius r_0: a radial wind with constant 4-speed V_0, proper density ρ_0, and magnetic field strength b_0. The initial isodensity contour is therefore spherical. Any distortion in the subsequent isodensity contours in the cold wind will be due solely to the frozen-in toroidal field because, in its absence,

the isodensity contours remain spherical. The initial (magnetic) Mach number M_0, which is equal to $(4\pi\rho_0)^{1/2}V_0/b_0$, is also a constant. Since the initial flow must be supermagnetosonic in order to apply the method of characteristics, we demand that $M_0 > 1$. If M_0 is much larger than one, however, the magnetic field will be too weak to collimate the wind effectively (Eichler 1993; § 3.3). If, on the other hand, M_0 is too close to one, then the poloidal magnetic field may not be negligible compared to the toroidal field, as assumed here. For these reasons, we shall always adopt $M_0 = 2$ unless noted otherwise.

Wind boundary conditions are required both on the equatorial plane and near the rotation (i.e., z-) axis. For the former, we can simply demand that one streamline lie exactly on the ϖ-axis. The latter boundary is more subtle to treat. Mathematically, we need to exclude a zone around the z-axis because the assumptions (of pure toroidal magnetic field and pure poloidal velocity) used in deriving equations (6)–(9) break down close to the z-axis (§ 3.4). Physically, a medium different from the MHD wind under consideration may exist in the axial region. In the case of young stellar objects, this medium could either be an ordinary stellar wind (Shu et al. 1988) or a bunch of open stellar magnetic field lines (Ostriker & Shu 1995). In any case, we assume that our supermagnetosonic winds are supported from within by a somewhat ad hoc medium, whose pressure distribution is prescribed by a simple power law ($\propto \varpi^{-P}$) for simplicity (SNOS). The pressure balance condition then yields

$$\gamma b \propto \varpi^{-P/2} , \tag{15}$$

at the wind/medium interface. Because of shearing, instabilities may occur at the interface and perhaps throughout the wind. Although such instabilities may be important in understanding how the dense (jet) parts of the wind are "lit up," we shall ignore this added complication here. To accommodate different situations, we shall leave the exponent P free to specify. If the open poloidal magnetic field provides the support, as assumed by SNOS, then $P = 4$. The exponent P, together with the angle θ_0 (between the rotation axis and the line drawn from the origin through the interface point on the initial sphere), specifies the inner wind boundary completely.

3.2. *Examples of Jet Formation*

We shall carry out our numerical construction of wind solutions in a meridional (or $\varpi - z$) plane. To cast the solution characteristic equations into dimensionless form, we scale length, density, and magnetic field by r_0, ρ_0, and b_0, respectively. We consider in turn jet formation in nonrelativistic, modestly relativistic, and highly relativistic MHD winds. They are represented by three choices of the initial 4-speed, $V_0 = 10^{-3}$, 2, and 5, respectively. For these examples, $\theta_0 = 20°$ and $P = 2.5$ are adopted for definitiveness.

The numerical procedure for constructing the supermagnetosonic wind solution using the "method of characteristics" is quite similar to that of LS, who treated the flow region between an oblique shock and a rigid wall (or flared disk). Their procedure is documented in detail in the Appendix of LS. The main differences are that, in the present problem, (a) the oblique shock is replaced by a free pressure boundary and (b) the flared disk is replaced by the equatorial plane. The numerical treatment of the free boundary is similar to that of the rigid wall except that, instead of the flow direction ϑ, it is the toroidal field strength b that is prescribed. The toroidal field is fixed according to the pressure balance equation (15). In addition, (c) we initiate our solution from a circle of given radius, instead of a cusp point (where the disk and the shock intercept in LS). Numerically, a set of discrete points along the initial circle is chosen, from which a network of plus and minus Mach lines are initiated and followed to greater and greater distances. Flow quantities are determined at each of the node points where the plus Mach lines intersect the minus Mach lines (interior points) and where the Mach lines intersect either the equator (wall points) or the wind/medium interface. The accuracy of these flow quantities is controlled mainly by the spacing between the starting points chosen on the initial circle. The smaller the spacing is, the more accurate the numerical calculation will be. However, more steps are then needed to march the solution to a given distance from the starting points. In the numerical examples shown below, we shall start with 50 points of equal spacing, which allows us to march the wind solution to a radius of order 10^4 times the initial radius with reasonable accuracy. One indicator of the accuracy of the marching is the smoothness of the streamlines and the isodensity contours that we shall derive through interpolation of the flow quantities obtained at the node points. We find that these solutions change little when the number of starting points is doubled to 100.

Let us first consider the nonrelativistic case with $V_0 = 10^{-3}$, which corresponds to a speed of 300 km s^{-1} (on the order of those inferred for jets/winds associated with T Tauri stars; Edwards, Ray, & Mundt 1993). The numerically determined wind streamlines and isodensity contours for this case are plotted in Figures 1*a*–1*d* on increasingly larger scales. On the smallest scale (Fig. 1*a*), we can see clearly how the initially spherical isodensity contours get more and more elongated along the rotation axis at larger and larger distances. The elongation starts from close to the interface, where the streamlines are collimated most quickly. The collimation of streamlines and the elongation of the isodensity contours occur simultaneously, both of which result from the pinching of the frozen-in toroidal magnetic field: in the absence of this field, a cold, spherical wind would remain spherical. The density decreases monotonically outward, and every three contours in the figures correspond to an order of magnitude drop in density. At still larger distances (Figs. 1*b* and 1*c*), as more and more streamlines are brought gradually toward the axis by toroidal magnetic pinching, the isodensity contours become more or less parallel to the rotation axis (and thus jetlike). The jetlike appearance of the isodensity contours is especially clear on the largest scale shown (Fig. 1*d*). By the time the last contour is reached, the density has dropped by six orders of magnitude. We should point out that the small ripples on the isodensity contours are purely numerical artifacts. Notice also that our isodensity contours in Figures 1*c* and 1*d* are qualitatively similar to those plotted in Figures 3*b* and 3*c* of SNOS, suggesting that the initially spherical isodensity contours in our case are trying to relax, under the influence of the toroidal magnetic field, toward their natural asymptotic state found by SNOS, in which the isodensity contours are nearly parallel to the rotation axis.

To put the above solution in a physical perspective, we first note that, for typical winds from T Tauri stars, the hydrogen number density at the initial isodensity contour is

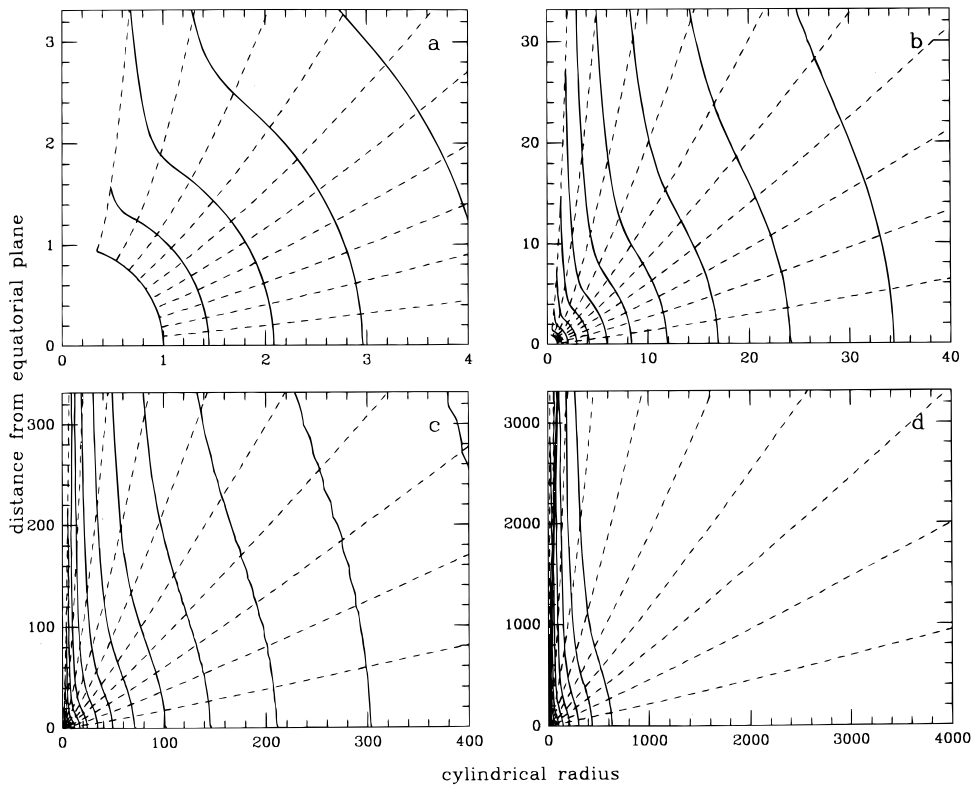

FIG. 1.—The streamlines (*dashed*) and the isodensity contours (*solid*) in a representative nonrelativistic MHD wind with an initial dimensionless 4-speed of $V_0 = 10^{-3}$ are plotted on increasingly large scales from panel (*a*) to panel (*d*). The initially circular isodensity contour (panel *a*) becomes increasingly more jetlike on larger and larger scales, as the streamlines get more and more collimated by the frozen-in toroidal magnetic field. The streamlines divide the wind into 10 regions of equal mass flux. The wind density decreases outward by a factor of 10 over every three isodensity contours. By the time the last contour on panel (*d*) is reached, the density has only 10^{-6} times its initial value.

about

$$n_{\rm H} = \frac{\dot{M}_w}{4\pi r_0^2 V_w \mu_{\rm H} m_p} \simeq \frac{5.4 \times 10^9}{\mu_{\rm H}} \left(\frac{\dot{M}_w}{3 \times 10^{-8}\ M_\odot\ {\rm yr}^{-1}} \right) \times \left(\frac{300\ {\rm km\ s}^{-1}}{V_w} \right) \left(\frac{0.05\ {\rm AU}}{r_0} \right)^2 {\rm cm}^{-3}\,, \quad (16)$$

where $\dot{M}_w$ is the total mass flux of the wind, V_w is the flow speed and $\mu_{\rm H}$ is the mean molecular weight in units of m_p. In the context of the X-celerator model of Shu et al. (1994), where the ratios in brackets are typically of order unity, we expect the initial number density to be of order a few times 10^9 cm^{-3}. In this case, the "jet" delineated by the last isodensity contour in Figure 1*d* has a number density of order 5×10^3 cm^{-3} and a half-width of order 20 AU. As noted by SNOS, such a number density is typical of the preshock values in shock models for optical jets (Hartigan, Morse, & Raymond 1994). In this particular example, about 25% of the total wind mass flux is concentrated within the "jet" on the scale of Figure 1*d*. We expect this fraction to increase logarithmically on still larger scales. On the scale of Figure 1*d*, about a third of the mass flux lies within 45° of the equatorial plane. This supports the general conclusion of SNOS that a well-collimated "jet" is always surrounded by a less-collimated (i.e., wide-angle) wind component. The interaction of the wide-angle wind with flared disks has been studied by LS. The fact that the Mach number in the presence of the toroidal field is on the order of only several ($M = 3.9$, 4.0, and 4.3 on the last three streamlines at $\varpi = 4000$ in this example), much smaller than that of typical *nonmagnetized* winds (Hartmann & Raymond 1989), has strong implications for the resultant wind-disk shocks (LS). Furthermore, when contained by a more or less isotropic external medium, we expect the dense, collimated "jet" part to escape to much larger distances than the wide-angle wind component.

Jets can be formed in the supermagnetosonic region of relativistic MHD winds as well, at least when the wind 4-speed is modest. We demonstrate this by repeating the above calculation with $V_0 = 2$ while keeping all other parameters the same as before. The results are shown in Figure 2. The overall appearance of the streamlines and isodensity contours in this relativistic case is quite similar to the nonrelativistic case: namely, the initially radial streamlines are gradually deflected toward the rotation axis, and the initially spherical isodensity contours become more and more elongated (and thus more and more jetlike) on larger and larger scales. The main difference is that, compared with Figure 1, the streamline collimation is more gradual, as evidenced by the fact that there are four streamlines intercepting the right-hand side of the frame of Figure 2*b* instead of three in Figure 1*d*. As a result, on the scale of Figure 2*b* (which is the same as Fig. 1*d*), a smaller fraction of the total wind mass flux (about 5% instead of 25% in Fig. 1*d*) is concentrated within the "jet" delineated by the last isodensity contour. To show the full extent of the last few isodensity contours, we have stretched the vertical coordinate of Figure 2*b* to 30,000 and shrunk the horizontal coordinate to 700 in Figure 2*c*. The more or less straight part of the "jet" is very narrow indeed: it has a length-to-half-width ratio of more than 100! We should point out that the

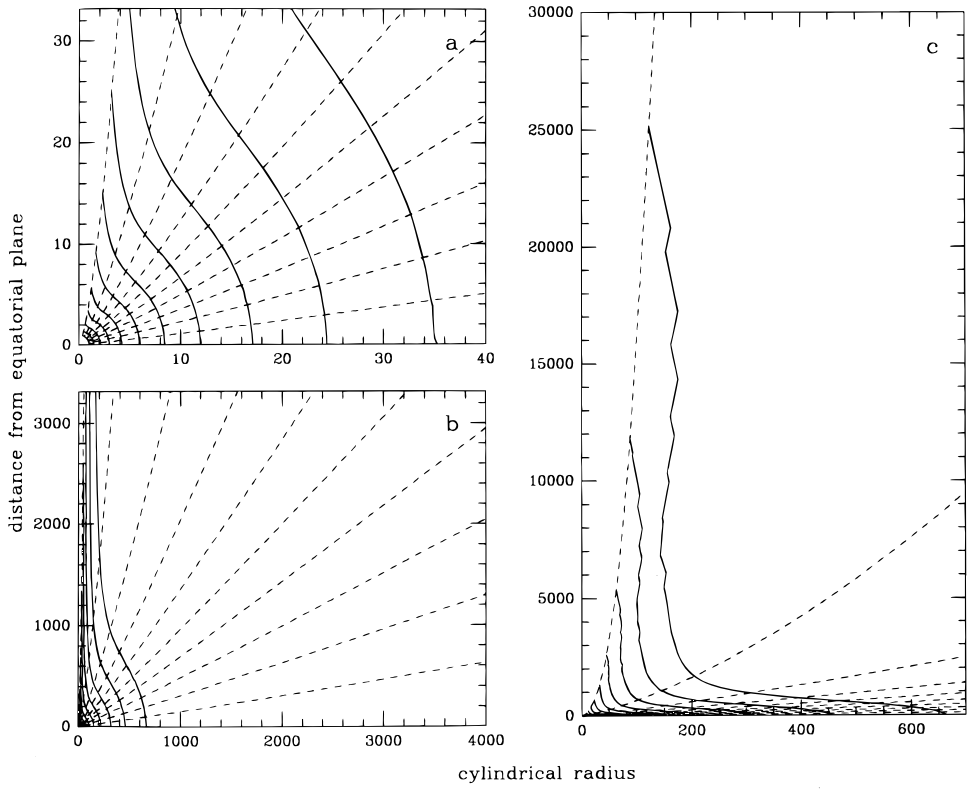

FIG. 2.—Jet formation in a modestly relativistic MHD wind with an initial dimensionless 4-speed of $V_0 = 2$. The coordinates in panel (*c*) are stretched to show the full extent of the last few isodensity contours, whose length-to-half-width ratios are on the order of 10^2.

contours are for the *proper* density ρ instead of the lab density $\gamma\rho$, which should not be much different: the largest wind Lorentz factor γ along each streamline in the figures is about 4 near the axis and about 3 in the equatorial region. Therefore, we conclude that jets can indeed be formed in modestly relativistic MHD winds with a Lorentz factor of a few, although the fraction of the total mass flux in the jet may be small.

As the wind Lorentz factor increases, it becomes increasingly difficult to form narrow "jets." We have computed a more relativistic case with $V_0 = 5$, while keeping all other parameters the same as before. The isodensity contours in this case remain nearly spherical up to a scale of 10^3 times the initial radius (where we terminated the calculation). The density has decreased by more than six orders of magnitude from its initial value. Although the density contours might eventually become more elongated on still larger scales, at this stage, they do not appear jetlike at all. It turns out that this and other aspects of jet formation in MHD winds can be understood qualitatively in terms of force balance across the streamlines, as we show below.

3.3. *Cross-Streamline Force Balance and Jet Formation*

Cross-streamline force balance is the key to understanding the jet-formation process in an initially spherical MHD wind for a simple reason: force must be exerted on the streamlines in the cross-streamline direction in order to bend them into a jet. Mathematically, this is expressed by the cross-streamline momentum equation

$$\kappa(M^2 + V^2) = -\boldsymbol{e}_c \cdot \frac{\nabla(b\varpi)}{b\varpi} \qquad (17)$$

where $\boldsymbol{e}_c$ is the unit vector in the cross-streamline direction pointing toward the rotation axis and $\kappa = \boldsymbol{e}_c \cdot (\boldsymbol{V} \cdot \nabla)\boldsymbol{V}/|\boldsymbol{V}|^2$ is the curvature of the streamline (Li, Chiueh, & Begelman 1992). The curvature characterizes the bending rate of a streamline since $\kappa = d\vartheta/dS$, where ϑ is the angle between the instantaneous direction of the streamline and the ϖ axis, and S is the coordinate along the streamline. Equation (17) tells us that it is proportional to the gradient of the product $b\varpi$ in the cross-streamline direction, which represents a combination of the magnetic pressure gradient and the magnetic tension force. From the Biot-Savart law, this product at each point of the wind is related to the poloidal electric current, I_p, enclosed within a circle of cylindrical radius ϖ through that point via $b\varpi = 2I_p/(\gamma c)$. Therefore, the condition for bending streamlines toward the rotation axis (to form a jet) is that the modified current, I_p/γ, increase across the streamlines toward the equator. This is not surprising because, for nonrelativistic winds ($\gamma = 1$), it is the $\boldsymbol{j} \times \boldsymbol{B}$ ($= j_p B \boldsymbol{e}_p \times \boldsymbol{e}_\phi = j_p B \boldsymbol{e}_c$, where $\boldsymbol{e}_p$ is the unit vector along a poloidal streamline) force that bends the streamlines. For a positive toroidal field (i.e., $B > 0$, implying a rotation vector in the negative z-direction), we thus demand that the poloidal current density j_p be greater than zero, which is equivalent to the above condition for the current I_p. The γ factor in the condition takes into account of the electric force, which is in the cross-streamline direction (eq. [4]). In the special case of a radial wind ($\kappa = 0$ therefore) with a constant $b\varpi$ everywhere, the cross-streamline force balance is satisfied exactly. In this case, the shape of the wind isodensity contours depends only on the distribution of the flux-to-mass ratio $F = b/(\rho\varpi)$, which is conserved along each streamline (eq. [12]). If the ratio F is also constant over all streamlines, then the contours of constant

density $\rho = [(b\varpi)/F]\varpi^{-2}$ will be cylinders (LS). This simple, exact solution demonstrates that, although the streamlines are perfectly radial, the wind can still appear jetlike. If, on the other hand, F increases with the angle ϑ (between the streamline and the ϖ axis) as $\sec^2 \vartheta$, the isodensity contours will be spherical.

With equation (17), we can now understand, at least qualitatively, why jets are formed in the first two of our three numerical examples (§ 3.2). Since the (proper) field strength b_0 is held constant across the streamlines initially and the cylindrical radius ϖ_0 increases toward the equator along the initial circle, there exists a gradient (pointing toward the equator) in the product $b_0\varpi_0$. This initial gradient is partially responsible for bending the streamlines toward the z-axis and elongating the initially spherical isodensity contours into jetlike shapes as shown in Figures 1 and 2. Jet formation in these examples is also aided by the inner boundary condition we prescribed on the wind/medium interface: we have adopted $P = 2.5$ in equation (15) so that $b\varpi \propto \varpi^{1-(P/2)}$ decreases with cylindrical radius ϖ along the interface. This reduction in $b\varpi$ helps to attract streamlines toward the inner boundary. To separate this effect from those due to the initial gradient in $b_0\varpi_0$, we hold $b_0\varpi_0$ constant and repeat the first example (from Fig. 1). The resulting streamlines and isodensity contours (with the same $P = 2.5$) are plotted in Figure 3*a*. For comparison, another case with $P = 2.8$ (so that $b\varpi$ decreases with radius ϖ slightly faster along the interface) is shown in Figure 3*b*. In both cases, spiky elongation of isodensity contours is evident, with the region closest to the wind/medium interface affected most.

Jets can form even without the help from the inner boundary condition, however. We demonstrate this by repeating the first example (Fig. 1) with $P = 2$ (so that $b\varpi$ remains constant along the interface) instead of $P = 2.5$. The resulting streamlines and isodensity contours (with the same constant initial b_0 as in Fig. 1) are plotted in Figure 3*c*. For comparison, another case with constant initial distribution of the magnetic-to-mass flux ratio $F_0 = b_0/(\rho_0\varpi_0)$ (which is in fact closer to the distribution adopted in the numerical example of SNOS), instead of b_0, is shown in Figure 3*d*. In both cases, the isodensity contours appear more or less parallel to the z-axis at large distances, indicating that jets are formed. It is only when the quantity $b\varpi$ is held constant both along the interface and across the streamlines will the initially spherical isodensity contours remain spherical (in agreement with the second exact wind solution mentioned earlier).

Finally, we discuss why jets are difficult to form in highly relativistic MHD winds. Using the identity $\kappa = d\vartheta/dS$, we recast equation (17) into

$$\frac{d\vartheta}{d\ln S} = \frac{-Se_c \cdot \nabla[\ln(b\varpi)]}{M^2 + V^2}, \tag{18}$$

which implies that the variation of the streamline angle ϑ is indeed logarithmically slow in general, unless the distance scale in the cross-streamline direction over which $b\varpi$ varies

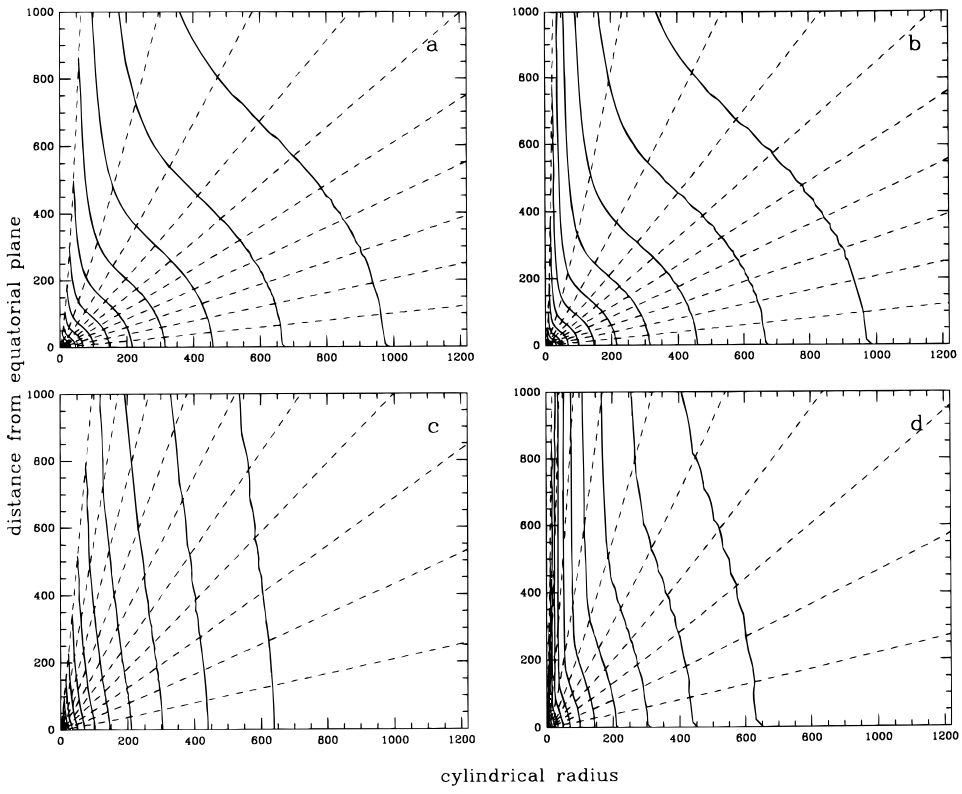

FIG. 3.—Effects of the inner boundary conditions (characterized by P in eq. [15]) and the initial distribution of the product $b\varpi$ ($\propto \varpi_0^Q$) on jet formation with $V_0 = 10^{-3}$, as in Fig. 1 (which has $P = 2.5$ and $Q = 1$). Shown in different panels are cases with various combinations of P and Q: (*a*) $P = 2.5$ and $Q = 0$; (*b*) $P = 2.8$ and $Q = 0$; (*c*) $P = 2$ and $Q = 1$; and (*d*) $P = 2$ and $Q = 2$. Panels (*a*) and (*b*) illustrate the "sucking" effects of the inner boundary when the external pressure drops faster than ϖ^{-2}. Panels (*c*) and (*d*) demonstrate the jetlike elongation of the isodensity contours due to magnetic pinching when $Q > 0$. A constant density at the initial radius of $r = 1$ is assumed on all streamlines in each panel. The initial distribution of the (magnetic) Mach number $M_0 = (4\pi\rho_0)^{1/2}V_0/b_0 \propto \varpi^{1-Q}$ is constant only in panel (*c*), however. We have adopted a minimum value of 2 for M_0 in the other three panels.

$\{=|e_c \cdot \nabla[\ln(b\varpi)]|^{-1}\}$ is much smaller than S. To deflect a streamline by a given angle, $\Delta\vartheta$, the coordinate S must increase by a factor of

$$\frac{S}{S_0} \simeq \exp\left\{\frac{(M^2 + V^2)\Delta\vartheta}{S|e_c \cdot \nabla[\ln(b\varpi)]|}\right\}. \quad (19)$$

Since M is of order unity initially, this factor is much larger for highly relativistic winds ($V \gg 1$) than for either nonrelativistic ($V \ll 1$) or modestly relativistic ($V \sim 1$) winds. Equation (19) illustrates the basic difficulty associated with jet formation in highly relativistic MHD winds, although it does not prevent jets from forming closer to the source, perhaps in the submagnetosonic region where both M and V can be small. It also implies that flow collimation is extremely hard to achieve once the Mach number becomes sufficiently large, as first pointed out by Eichler (1993). As a result, the (magnetic) Mach number in MHD winds should remain moderate even on relatively large scales, in agreement with our first example.

3.4. *Discussion of Assumptions*

We now comment on the simplifications made in the above treatment of the jet-formation problem in MHD winds. First of all, we have ignored both the poloidal (denoted by subscript "p" below) magnetic field and the toroidal (denoted by subscript "ϕ" below) flow speed in the MHD winds. To determine the conditions under which these approximations are valid, we shall make use of some general properties of MHD winds. For nonrelativistic winds, there exists a so-called "Alfvén radius," $\varpi_A = (l/\Omega)^{1/2}$ (where l and Ω are the conserved total specific angular momentum and rotation rate along a given field line; e.g., Pudritz 1988), beyond which $V_p \approx \varpi_A\Omega$ and $V_\phi \lesssim \varpi_A^2\Omega/\varpi$. In this region, the flux-freezing condition yields $B_p/(-B_\phi) = V_p/(\Omega\varpi - V_p) \approx V_p/(\Omega\varpi) \approx \varpi_A/\varpi$. Therefore, we should be able to neglect B_p compared with B_ϕ when $\varpi \gg \varpi_A$. The condition for ignoring the centrifugal force associated with V_ϕ (compared with magnetic forces associated with the toroidal field) is $4\pi\rho V_\phi^2/B_\phi^2 \ll 1$. This corresponds to the condition $\varpi/\varpi_A \gg M > 1$ in the supermagnetosonic region that interests us, where $M^2 = 4\pi\rho V_p^2/B_\phi^2$ is the (magnetic) Mach number defined earlier. For relativistic winds ($V_p \approx c$), the flux-freezing condition beyond the so-called "light cylinder radius," $\varpi_L = c/\Omega$ (e.g., Li et al. 1992), yields $B_p/(-B_\phi) = V_p/(\Omega\varpi - V_\phi) \approx c/(\Omega\varpi) = \varpi_L/\varpi$. Therefore, we need to demand $\varpi \gg \gamma\varpi_L$ in order to neglect B_p compared with the *proper* toroidal field, B_ϕ/γ. Furthermore, from the relation $V_\phi/V_p \lesssim \varpi_L/\varpi$, we find that the toroidal speed can be ignored when $\varpi \gg M\varpi_L$. All together, we conclude that a sufficient condition for ignoring both B_p and V_ϕ is that the cylindrical radius $\varpi \gg \max(\gamma, M)\varpi_c$, where ϖ_c stands for the Alfvén radius for nonrelativistic winds and the light cylinder radius for relativistic winds. It is in principle possible to include both B_p and V_ϕ in our formulation. However, such inclusion is laborious and we do not think that it could affect our conclusions regarding jet formation much for the following reason: although forces associated with B_p and V_ϕ may become comparable to those associated with B_ϕ close to the starting location, they die away with radius much ($\propto \varpi^{-2}$ times) more quickly. Jet formation, being a slow process spanning decades in radii (Fig. 1), should not be affected much.

In addition, we have assumed idealized starting conditions, i.e., radially directed, supermagnetosonic winds with constant flow speed and density on an initial sphere. In the absence of general transmagnetosonic wind solutions, we feel that more complicated choices are unwarranted at the present time. Jets might actually form more easily when allowance is made for the tendency for wind isodensity contours to become somewhat elongated (along the z-axis) even before the supermagnetosonic region is reached (Sakurai 1985; Najita & Shu 1994). Although the degree of such elongation is hard to quantify in general, it is expected to facilitate the process of jet formation discussed in this paper. Finally, we reiterate that our inner wind boundary is uncertain. We have inserted a somewhat ad hoc pressurized medium to prevent the wind from crashing onto the rotation axis (and invalidating our solutions). Fortunately, although a rapid decrease in pressure along the inner boundary (i.e., $P > 2$ in eq. [15]) can help jet formation, it is not required, as long as an initial (outward) gradient of the product $b\varpi$ exists across the streamlines (Figs. 3*c* and 3*d*). The fact that jets are formed even when the product $b\varpi$ remains constant along the boundary (i.e., $P = 2$) gives us confidence about the robustness of jet formation in MHD winds.

4. SUMMARY AND DISCUSSION

Frozen-in toroidal magnetic fields in MHD winds have long been invoked to produce narrow "jets" associated with both active galactic nuclei and young stellar objects (e.g., Begelman et al. 1984; Königl & Ruden 1993). In this paper, we test this idea in the supermagnetosonic region of MHD winds, where flow solutions can be constructed readily using the well-known "method of characteristics" once initial and boundary conditions are prescribed. We have chosen a simple condition on an initial sphere: a radially streaming flow with uniform density distribution. The initially spherical isodensity contour allows us to follow the jet formation most clearly, since this process is most apparent from the isodensity contours at increasingly large scales (SNOS; Fig. 1).

The main conclusion of the paper is that jetlike isodensity contours could indeed arise naturally in the supermagnetosonic region of nonrelativistic or modestly relativistic MHD winds. These contours are elongated along the axis in the process of gradual streamline collimation, which results from a force imbalance in the cross-streamline direction. In the absence of both thermal pressure (i.e., in a cold wind) and rotation, the only forces available are the magnetic pressure gradient and tension. We therefore conclude that toroidal magnetic field, which is the only field component present in this study, is responsible for producing the jets shown in Figures 1–3.

The frozen-in toroidal field can cause wind collimation directly by squeezing the streamlines toward the axis with a combination of magnetic pressure and tension forces. This combined force is proportional to the gradient of the product of the proper field strength (b) and the cylindrical radius (ϖ). If the initial condition is so arranged that $b\varpi$ decreases across streamlines toward the axis, then there exists a net magnetic force which tries to collimate the wind. Since the quantity $b\varpi$ is conserved along a *radial* streamline (from mass conservation and flux-freezing), the collimating force will persist unless some degree of collimation is achieved. In this case, jets are formed to release the magnetic stresses in the cross-streamline direction built in by the prescribed initial condition.

Because toroidal magnetic field supplies the pressure of the wind, it can also affect the wind collimation through pressure balance across the inner boundary near the axis. If the external pressure in the axial region drops (with cylindrical radius) fast enough, then the magnetic pressure in the wind will collimate the boundary (i.e., innermost wind streamline). This collimation in turn "sucks" the outer streamlines toward the axis, and thus facilitating jet formation.

Jets formed in supermagnetosonic MHD winds have two salient features: (1) they are always surrounded by a wide-angle wind component, as first pointed out by SNOS. This wide-angle MHD wind component may drive the molecular bipolar outflows associated with many young stellar objects (e.g., Li & Shu 1996b); (2) they have a (magnetic) Mach number of order several on astrophysically relevant scales. The latter feature can be understood in terms of the cross-streamline force balance equation (17). This equation also shows that jet formation is much more difficult in highly relativistic, supermagnetosonic MHD winds. It is therefore not surprising that the Crab pulsar wind, which is believed to be ultrarelativistic (e.g., Kennel & Coroniti 1984), does not appear predominantly jetlike.

I thank F. H. Shu for informative discussions and encouragement and F. Wilkin and an anonymous referee for suggestions which improved the presentation of the paper. This research is supported by the Theoretical Astrophysics Center at University of California at Berkeley.

REFERENCES

Begelman, M. C., Blandford, R. D., & Rees, M. J. 1984, Rev. Mod. Phys., 56, 265
Begelman, M. C., & Li, Z.-Y. 1994, ApJ, 426, 269
Blandford, R. D. 1989, in Theory of Accretion Disks, ed. F. Meyer et al. (Dordrecht: Kluwer), 35
Blandford, R. D., & Payne, D. G. 1982, MNRAS, 199, 883
Burrows, C. J., et al. 1996, preprint
Carilli, C. L., Perley, R. A., Bartel, N., & Sorathia, B. 1996, in Energy Transport in Radio Galaxies & Quasars, ed. P. Hardee, A. Bridle, & A. Zensus, in press
Chiueh, T., Li, Z.-Y., & Begelman, M. C. 1991, ApJ, 377, 462
Edwards, S., Ray. T., & Mundt, R. 1993, in Protostars and Planets III, ed. E. H. Levy & J. H. Lunine (Tucson: Univ. Arizona Press), 567
Eichler, D. 1993, ApJ, 419, 111
Hartigan, P., Morse, J. A., & Raymond, J. 1994, ApJ, 436, 125
Hartmann, L., & Raymond, J. C. 1989, ApJ, 337, 903
Heyvaerts, J., & Norman, C. 1989, ApJ, 347, 1055
Kennel, C. F., & Coroniti, F. V. 1984, ApJ, 283, 694
Königl, A., & Ruden, S. P. 1993, in Protostars and Planets III, ed. E. H. Levy & J. H. Lunine (Tucson: Univ. Arizona Press), 641
Lada, C. J. 1985, ARA&A, 23, 267
Li, Z.-Y., Chiueh, T., & Begelman, M. C. 1992, ApJ, 394, 459
Li, Z.-Y., & Shu, F. H. 1996a, ApJ, 468, 261 (LS)
———. 1996b, ApJ, in press
Lovelace, R. V. E., Mechanian, C., Mobarry, C., & Sulkanen, M. E. 1986, ApJS, 62, 1
Mundt, R. 1985, in Protostars and Planets II, ed. D. C. Black & M. S. Mathews (Tucson: Univ. Arizona Press), 414
Najita, J., & Shu, F. H. 1994, ApJ, 429, 808
Ostriker, E. C., & Shu, F. H. 1995, ApJ, 429, 813
Pudritz, R. 1988, in Galactic and Extragalactic Star Formation, ed. R. Pudritz & M. Fich (Dordrecht: Kluwer), 135
Sakurai, T. 1985, A&A, 152, 121
Shu, F. H. 1992, The Physics of Astrophysics, Vol. II (Mill Valley: University Science Books)
Shu, F. H., et al. 1994, ApJ, 429, 781
Shu, F. H., Lizano, S., Ruden, S. P., & Najita, J. 1988, ApJ, 328, L19
Shu, F. H., Najita, J., Ostriker, E. C., & Shang, H. 1995, ApJ, 455, L155 (SNOS)
Tomimatsu, A. 1994, PASJ, 46, 123
Zucrow, M. J., & Hoffman, J. D. 1977, Gas Dynamics, Vol. II (New York: Wiley)